Estimation of Tokamak Plasma Position and Shape in TOKASTAR-2 Using Magnetic Field Measurement*)

Kouhei YASUDA, Hideki ARIMOTO, Atsushi OKAMOTO, Takaaki FUJITA, Masato MINOURA, Ryoma YOKOYAMA and Takahiro YAMAUCHI

Graduate School of Engineering, Nagoya University, Furo-cho, Chikusa-ku, Nagoya 464-8603, Japan

(Received 28 December 2017 / Accepted 7 May 2018)

The tokamak plasma position and shape were estimated for the first time in TOKASTAR-2 based on external magnetic measurement using filament current approximation method. Data of a magnetic probe array and flux loops was used. Effects of the helical field on the tokamak plasma radial position were investigated. The oscillation of the radial position and the outer displacement of the plasma under the weak vertical field were suppressed by the helical field.

Keywords: helical field application, TOKASTAR, magnetic measurement, plasma position and shape

DOI: 10.1585/pfr.13.3402072

1. Introduction

Helical field is thought to provide improved positional stability and the stabilization of the plasma position by applying the helical field to the tokamak plasma was shown [1, 2]. A tokamak-stellarator hybrid confinement called 'TOKASTAR' was proposed [3], which is a compact system with a low aspect ratio ($A < 3$) and has simple helical coils. TOKASTAR-2 is a hybrid plasma confinement device based on TOKASTAR concept [4]. One of the main purposes of TOKASTAR-2 is to study the stabilization effect of the tokamak plasma position by applying the helical field of the simple helical coils.

Figure 1 shows the coil systems of TOKASTAR-2. Tokamak and stellarator coil systems can be operated independently or simultaneously. The stellarator coil system consists of two HF (Helical Field) coils in parallelogram shape, four AHF (Additional Helical Field) coils in fan shape and two circular VF (Vertical Field) coils. These coils are connected to DC power supplies. The HF coils are located outside in the radial direction while the AHF coils are located on upper and lower sides. They were designed so that the magnetic surfaces are generated without the plasma current. The tokamak coil system consists of three-block OH (Ohmic Heating) coils and two PVF (Pulse Vertical Field) coils. The PVF coils are used to generate a varying vertical field for the tokamak equilibrium. Eight TF (Toroidal Field) coils and two SC (Shape Control) coils are commonly used for tokamak and helical operations but SC coils are not used in this study. The OH coils, the PVF coils and the TF coils are connected to pulsed power supplies with capacitor banks.

Figure 2 shows the stabilization of the tokamak plasma position by applying the helical field conceptually. The tokamak equilibrium of TOKASTAR-2 is shown in Fig. 2 (a) while the helical vacuum magnetic surface is shown in Fig. 2 (b). The effective axisymmetric poloidal field component of the helical field is in the same direction as the poloidal field generated by the plasma current when the rotational transform by the helical field and that by the plasma current are in the same direction. This effective

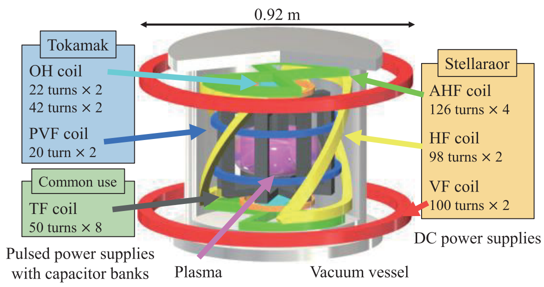

Fig. 1 Coil systems of TOKASTAR-2.

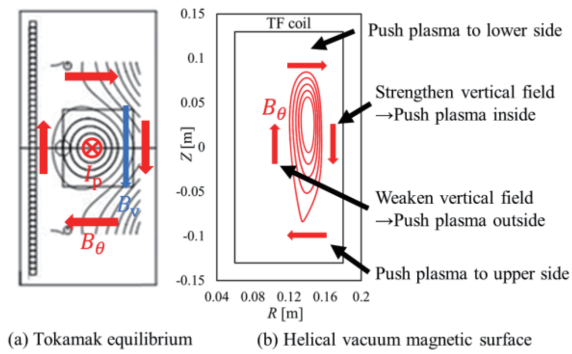

Fig. 2 Stabilization of the tokamak plasma position by applying the helical field.

---

author's e-mail: yasuda-kohei16@ees.nagoya-u.ac.jp

*) This article is based on the presentation at the 26th International Toki Conference (ITC26).

axisymmetric poloidal field pushed the plasma column toward the magnetic axis of the helical field through Lorenz force and then the stabilization effect on the plasma position is expected.

The effect of the helical field application on the plasma radial position was observed by an internal magnetic field measurement [5] and by a high-speed camera [6] in TOKASTAR-2. However, the plasma current and position were influenced by insertion of the magnetic probe in [5]. No precise position of the plasma was obtained in [6] since the camera image was based on light intensity integrated along the tangential sight lines. Moreover, it was difficult to estimate the tokamak plasma shape by these two methods. In this paper, using an external magnetic field measurement newly installed, the tokamak position and shape in TOKASTAR-2 are obtained without influence on the plasma. The effect of the helical field on the plasma radial position is investigated.

2. Measuring Methods

Figure 3 shows the location of magnetic sensors in TOKASTAR-2. A magnetic probe array (MPA) was installed in April 2017. The 16 sensor coils are located in ceramic rods for protection from the plasma. The rods are located along the TF coils. All sensor coils on the inner and outer sides and one sensor coil on the upper and lower sides (CH 5 and 13) measure the vertical magnetic field and two sensor coils on the upper and lower sides (CH 4, 6, 12 and 14) measure the radial magnetic field. The circuits of two sensor coils (CH 9 and 12) have become open and the other 14 sensor coils are used. The product of the number of turns N and the effective coil area S, NS, of the sensor coils is $2.49 \times 10^{-3}\,\mathrm{m}^2$. The resonant frequency of the sensor coils is $\sim 90\,\mathrm{kHz}$, which is high enough for measurement of the TOKASTAR-2 tokamak plasma whose duration time is $\sim 0.5\,\mathrm{ms}$. The magnetic field was obtained by numerically integrating the voltage of the sensor coils.

We also used four magnetic flux loops located at $R = 0.06\,\mathrm{m}$, $Z = \pm 0.13\,\mathrm{m}$ and $R = 0.18\,\mathrm{m}$, $Z = \pm 0.10\,\mathrm{m}$. The magnetic flux was also obtained by numerically integrating the voltage of the flux loops.

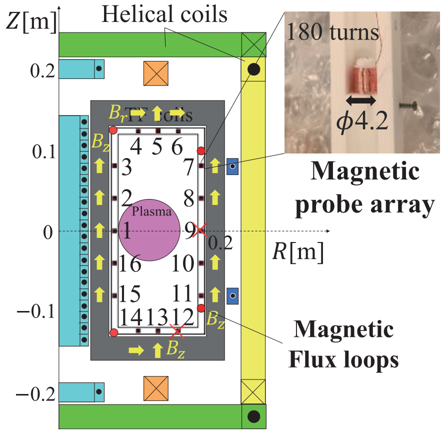

Fig. 3 Measuring instruments.

3. Method of Analysis

We used filament current approximation method [7] to estimate the tokamak plasma position and shape. The tokamak plasma shape is obtained from contours of the poloidal magnetic flux

$$\psi_{\mathrm{total}} = \psi_{\mathrm{p}} + \psi_{\mathrm{vac}}, \tag{1}$$

where ψ_{p} is magnetic flux generated by the plasma current and ψ_{vac} is that generated by the external coils current and the eddy current. We modeled the plasma current by the six ring filaments. In TOKASTAR-2, a large eddy current is driven in the vacuum vessel, which cancels the vertical field [8] and hence it is difficult to obtain ψ_{vac} by calculation. In this paper, ψ_{vac} is determined from the magnetic field $B_k^{\mathrm{vac,exp}}$ measured by MPA and the magnetic flux $\psi_j^{\mathrm{vac,exp}}$ measured by flux loops in the shot without plasma, where subscripts (k and i) denote the channel numbers of the sensors. The ψ_{p} is determined by the measured values of the poloidal magnetic field $B_k^{\mathrm{p,exp}}$ and the magnetic flux $\psi_j^{\mathrm{p,exp}}$ generated by the plasma current. We evaluate $B_k^{\mathrm{p,exp}}$ and $\psi_j^{\mathrm{p,exp}}$ by $B_k^{\mathrm{p,exp}} = B_k^{\mathrm{total,exp}} - B_k^{\mathrm{vac,exp}}$, $\psi_j^{\mathrm{p,exp}} = \psi_j^{\mathrm{total,exp}} - \psi_j^{\mathrm{vac,exp}}$, where $B_k^{\mathrm{total,exp}}$ and $\psi_j^{\mathrm{total,exp}}$ are the signal obtained in the tokamak discharge. Contribution from the difference in the PVF coils current and eddy current between the cases with and without the plasma is modeled by additional filaments located at the postion of the PVF coils.

3.1 Single filament

An initial guess of the plasma position, which is needed to locate the six filaments, is determined by modeling the plasma by a single ring filament. The filament current is fixed to the measured value of the plasma current, I_{p}. The residual sum of squares between the measured value and the calculated value

$$E_{1\mathrm{fila}} = \sum_{k=1}^{14} (B_k^{\mathrm{p,cal}} - B_k^{\mathrm{p,exp}})^2 + a_{\mathrm{p}} \sum_{j=1}^{4} (\psi_j^{\mathrm{p,cal}} - \psi_j^{\mathrm{p,exp}})^2, \tag{2}$$

is calculated for a single filament located at a grid point in the RZ plane. The grid spacing is 2 mm both in R- and Z- directions. The coefficient a_{p} is fixed to $10000\,\mathrm{T}^2/\mathrm{Wb}^2$. $B_k^{\mathrm{p,cal}}$ and $\psi_j^{\mathrm{p,cal}}$ are the calculated values of the poloidal magnetic field and magnetic flux, respectively. The number of summation for the first and second terms, 14 and 4 are the numbers of the field sensor coils and the flux loops, respectively. The position $(R_{1\mathrm{fila}}, Z_{1\mathrm{fila}})$ where $E_{1\mathrm{fila}}$ is minimized is determined and the six ring filaments are located around $(R_{1\mathrm{fila}}, Z_{1\mathrm{fila}})$.

3.2 Six filaments and additional filaments

The poloidal magnetic field and flux at sensors generated by unit current in the six ring filaments and two additional filaments are calculated. The following error

$$E_{\rm p}=\sum_{k=1}^{14}(B_k^{\rm p,cal}-B_k^{\rm p,exp})^2+a_{\rm p}\sum_{j=1}^{4}(\psi_j^{\rm p,cal}-\psi_j^{\rm p,exp})^2 + b_{\rm p}\sum_{i=1}^{8} I_i^2, \quad (3)$$

is minimized where I_i is filament currents. The third term is added to prevent the filament currents from being large. The coefficient $b_{\rm p}$ is adjusted so that $I_{1-6} > 0$ and $|\sum I_i - I_{\rm p}| \le I_{\rm p}\times 0.05$. Simultaneous equations on I_i, obtained from $\partial E_{\rm p}/\partial I_i = 0$, are solved. The position of the current centroid is then obtained by

$$R_{\rm centroid}=\frac{\sum_{i=1}^{6} R_i^{\rm f} I_i}{\sum_{i=1}^{6} I_i},\ Z_{\rm centroid}=\frac{\sum_{i=1}^{6} Z_i^{\rm f} I_i}{\sum_{i=1}^{6} I_i}, \quad (4)$$

where $(R_i^{\rm f}, Z_i^{\rm f})$ is the position of six filaments.

3.3 Vacuum magnetic field

We used multipole magnetic field to calculate $\psi_{\rm vac}$. By Maxwell equation, $\psi_{\rm vac}$ satisfies

$$\varDelta^*\psi_{\rm vac}=\frac{\partial^2\psi_{\rm vac}}{\partial R^2}-\frac{1}{R}\frac{\partial\psi_{\rm vac}}{\partial R}+\frac{\partial^2\psi_{\rm vac}}{\partial Z^2}=0. \quad (5)$$

The solution of Eq. (5) is expanded to multipole field including dipole, quadrapole, hexapole, octpole and decapole fields with even and odd modes. The $\psi_{\rm vac}$ is expressed by a linear combination of these fields

$$\psi_{\rm vac}=c_0+c_1\psi_{\rm di}^{\rm even}+c_2\psi_{\rm di}^{\rm odd}+\cdots. \quad (6)$$

To determine the coefficient c_l, residual sum of squares

$$E_{\rm vac}=\sum_{k=1}^{14}(B_k^{\rm vac,cal}-B_k^{\rm vac,exp})^2 + a_{\rm vac}\sum_{j=1}^{4}(\psi_j^{\rm vac,cal}-\psi_j^{\rm vac,exp})^2, \quad (7)$$

is minimized. Simultaneous equations on c_l, obtained from $\partial E_{\rm vac}/\partial c_l = 0$, are solved. The coefficient $a_{\rm vac}$ is fixed to $10000\,{\rm T^2/Wb^2}$. $B_k^{\rm vac,cal}$ and $\psi_j^{\rm vac,cal}$ are the calculated values of the vacuum magnetic field and magnetic flux, respectively.

4. Results

4.1 Tokamak plasma shape

Figure 4 shows the contour of the poloidal magnetic flux of the tokamak discharge at $t = 2.8$ ms which is close to the time of the plasma current peak. The charging voltages of capacitor banks for the PVF coils, the TF coils and the OH coils are $V_{\rm PVF} = 0.33$ kV, $V_{\rm TF} = 1.1$ kV and $V_{\rm OH} = 2.0$ kV. Nitrogen gas was used as working gas. The tokamak plasma position and shape were obtained for the first time in TOKASTAR-2. In this case, the plasma major radius $R = 0.111$ m, the plasma minor radius $a = 0.035$ m, the aspect ratio $A = 3.15$ and the elongation $\kappa = 0.96$. Figure 5 shows comparison between the measured value and the calculated value of (a) the magnetic field and (b) magnetic flux. The calculated values are consistent with the measured values.

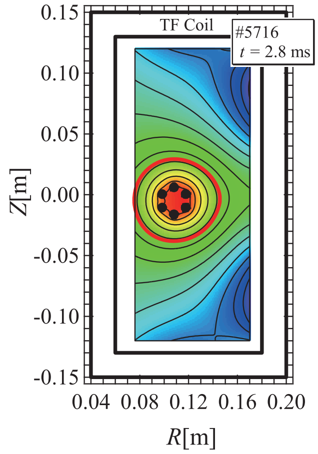

Fig. 4 Contour plot of poloidal flux. Red line is the last closed flux surface and black dots are six ring filaments.

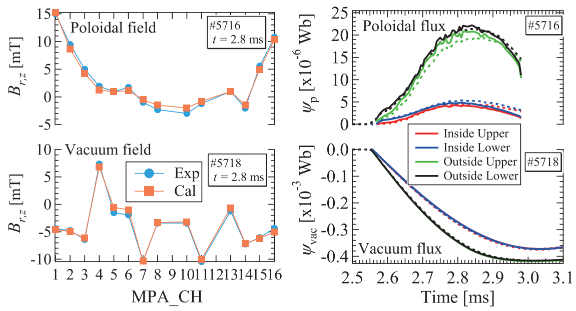

(a) magnetic field (b) magnetic flux

Fig. 5 Comparison between measured values and calculated values of the magnetic field and flux. In (a), the horizontal axis is the channel number of MPA. In (b), solid lines denote the calculated values and dotted lines denote the measured values.

4.2 Application of the helical field

To study the effect of the helical field, the external helical field was applied to the tokamak plasma. The $V_{\rm PVF}$ was scanned with constant $V_{\rm TF} = 1.1$ kV and $V_{\rm OH} = 2.0$ kV. The currents of the stellarator coil systems were $I_{\rm HF} = 2.5$ kAturn, $I_{\rm AHF} = 2.88$ kAturn, $I_{\rm VF} = 0.15$ kAturn by which closed magnetic surfaces were generated. Figure 6 shows time evolution of the plasma current $I_{\rm p}$ with and without the helical field for several values of $V_{\rm PVF}$. Figure 7 shows maximum of $I_{\rm p}$ as a function of the vertical field at $R = 0.12$ m at $t = 2.8$ ms when the PVF

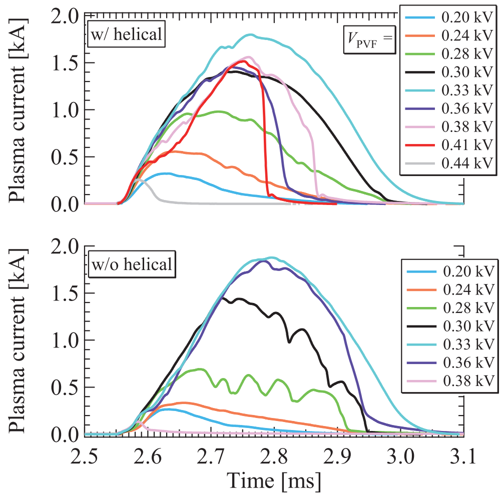

Fig. 6 The plasma current (top) with and (bottom) without the helical field.

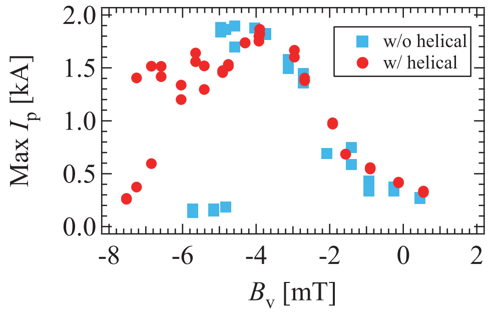

Fig. 7 The maximum of the plasma current as a function of the vertical field at R = 0.12 m at t = 2.8 ms.

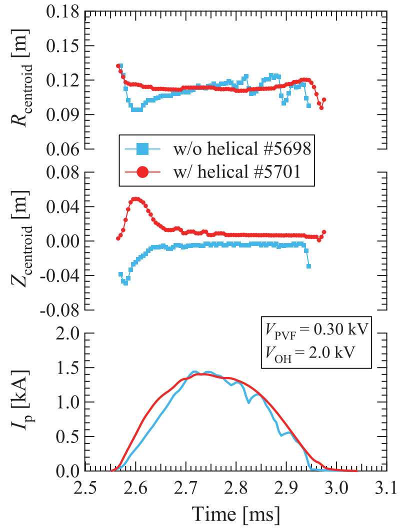

Fig. 8 Comparison between the positions of the current centroid with and without the helical field.

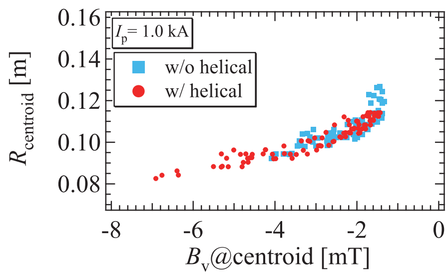

Fig. 9 The radial position as a function of the vertical field at I_p = 1.0 kA.

coils current becomes maximum. As shown in Fig. 7, the plasma current becomes ~1.9 kA around $B_v = -4$ mT both with and without the helical field. The plasma current was reduced drastically under the strong vertical field ($B_v < -5$ mT) for the case without the helical field. In contrast, the plasma current was reduced more gradually with the vertical field for the case with the helical field.

Figure 8 shows the time evolution of the position of the current centroid and of the plasma current with and without the helical field at V_{PVF} = 0.30 kV. The position of the tokamak plasma with the helical field was obtained ignoring the three-dimensionality of the plasma current distribution. The oscillation of the radial position observed in a shot without the helical field is suppressed by applying the helical field. Figure 9 shows the radial position as a function of the vertical field B_v (= B_{PVF}+B_{OH}+B_{eddy}) at the position of the current centroid for the specific plasma current (1.0 kA). The several data in V_{PVF} scan at V_{OH} = 1.6, 1.7, 1.8, 2.0 kV was analyzed. The outer displacement of the plasma under the weak vertical field $B_v \sim -1.5$ mT is observed in plasmas without the helical field, but it is suppressed in plasmas with the helical field. These results show that the tokamak plasma radial position is stabilized by applying the helical field for large plasma major radii, typically $R_{centroid} \sim 0.11$ m (radial positions of outer plasma edge > 0.145 m) under the weak vertical field. The effective vertical field of the helical field on the equator plane is weak (less than 0.2 mT) in a range 0.075 m < R < 0.145 m but it increases rapidly with R in a range R > 0.145 m. Quantitative valuation of the helical field needs more detailed analysis including averaging the effective vertical field over the plasma cross section. It is out of the scope of the present paper and is regarded as future work.

5. Summary

The tokamak plasma position and shape were estimated for the first time in TOKASTAR-2 by magnetic measurement and filament current approximation method. The poloidal magnetic flux generated by the plasma current was modeled by six ring filaments and the vacuum magnetic flux was modeled by multipole fields.

We investigated effects of the helical field on the tokamak plasma position. The oscillation of the radial position observed in a shot without the helical field is suppressed by applying the helical field. The outer displacement of the plasma under the weak vertical field was also suppressed by the helical field. The helical field by the simple helical coils contributes to the positional stability to the radial position in the tokamak plasma.

Acknowledgments

This work is performed with the support and under the auspices of the NIFS Collaboration Research program (NIFS14KOAP027, NIFS17KLEP026).

[1] K. Sakurai and S. Tanahashi, J. Phys. Soc. Jpn. **49**, 759 (1980).
[2] H. Ikezi, K.F. Schwarzenegger and C. Ludescher, Phys. Fluids **22**, 2009 (1979).
[3] K. Yamazaki and Y. Abe, Nagoya Research Report IPPJ-718 (1985).
[4] T. Oishi, K. Yamazaki, K. Okano *et al*., J. Plasma Fusion Res. SERIES **9**, 69 (2010).
[5] T. Ueda, H. Arimoto, T. Fujita *et al*., J. Plasma Fusion Res. **10**, 3402065 (2015).
[6] T. Sakito, H. Arimoto, T. Fujita *et al.*, Plasma Fusion Res. **11**, 2402074 (2016).
[7] D.W. Swain and G.H. Neilson, Nucl. Fusion **22**, 1015 (1982).
[8] R. Nishimura, H. Arimoto, T. Fujita *et al*., Plasma Fusion Res. **9**, 3402059 (2014).